

Proton NMR measurements of the local magnetic field in the paramagnetic metal and antiferromagnetic insulator phases of λ -(BETS)₂FeCl₄

Guoqing Wu,¹ P. Ranin,¹ W. G. Clark,¹ S. E. Brown,¹ L. Balicas,² and L. K. Montgomery³

¹*Department of Physics and Astronomy, UCLA, Los Angeles, California 90095-1547, USA*

²*National High Magnetic Field Laboratory, Florida State University, Tallahassee, Florida 32306, USA*

³*Department of Chemistry, Indiana University, Bloomington, IN 47405, USA*

(Dated: December 2, 2024)

Measurements of the ¹H-NMR spectrum are reported for a small ($\sim 4 \mu\text{g}$) single crystal of the organic conductor λ -(BETS)₂FeCl₄, with an applied magnetic field $\mathbf{B}_0 = 9 \text{ T}$ parallel to the *a*-axis in the *ac*-plane over a temperature (*T*) range 2.0 – 180 K. They provide the distribution of the static local magnetic field at the proton sites in the paramagnetic metal (PM) and antiferromagnetic insulator (AFI) phases, along with the changes that occur at the PM–AFI phase transition. The spectra have six main peaks that are significantly broadened and shifted at low *T*. The origin of these features is attributed to the large dipolar field from the 3d Fe³⁺ ion moments (spin $S_d = 5/2$). Their amplitude and *T*–dependence are modeled using a modified Brillouin function that includes a mean field approximation for the total exchange interaction (J_0) between one Fe³⁺ ion and its two nearest neighbors. A good fit is obtained using $J_0 = -1.7 \text{ K}$. At temperatures below the PM–AFI transition temperature $T_{MI} = 3.5 \text{ K}$, an extra peak appears on the high frequency side of the spectrum and the details of the spectrum become smeared. Also, the rms linewidth and the frequency shift of the spectral distribution are discontinuous, consistent with the transition being first-order. These measurements verify that the dominant local magnetic field contribution is from the Fe³⁺ ions and indicate that there is a significant change in the static local magnetic field distribution at the proton sites on traversing the PM to AFI phase transition.

PACS numbers: 75.30.Kz, 75.50.Ee, 76.60.-k, 71.30.+h

I. INTRODUCTION

The organic conductor λ -(BETS)₂FeCl₄, where BETS is bis(ethylenedithio)tetraselenafulvalene (C₁₀S₄Se₄H₈), is of considerable interest because of the properties related to the coexistence of the large magnetic 3d Fe³⁺ moments (spin $S_d=5/2$) of the inorganic anions (FeCl₄⁻) and the conduction π -electrons (spin $S_\pi=1/2$) in the donor molecules from the BETS.^{1,2,3,4,5,6} It has an unusual phase diagram, including an antiferromagnetic insulating (AFI) phase, a paramagnetic metallic (PM) phase, and a field-induced superconducting (FISC) phase.^{1,2}

The crystal structure of λ -(BETS)₂FeCl₄, shown in Fig. 1, is triclinic with the space group P $\bar{1}$ and the lattice constants at 298 K $a = 16.164(3) \text{ \AA}$, $b = 18.538(3) \text{ \AA}$, $c = 6.5928(8) \text{ \AA}$, $\alpha = 98.40(1)^\circ$, $\beta = 96.67(1)^\circ$, $\gamma = 112.52(1)^\circ$ and $V = 1773.0(5) \text{ \AA}^3$.^{3,7} There are four BETS molecules and two Fe³⁺ ions per unit cell and the BETS molecules are stacked along the *a*- and *c*-axes to form a quasi-stacking fourfold structure. The conducting layers, comprised of BETS, are sandwiched along the *b*-axis by the insulating layers of FeCl₄⁻ anions. The least conducting axis is *b*, *ac* is the conducting plane, and the easy axis of the antiferromagnetic spin structure is $\sim 30^\circ$ away from the *c* axis (|| needle axis of the crystal).⁸

A mechanism used to explain the FISC phase below 5 K in λ -(BETS)₂FeCl₄ is based upon the Jaccarino-Peter (J-P) compensation effect⁹ operating in a two-dimensional (2D) system.^{1,2,10,11} In this model, the negative exchange interaction ($J_{\pi d}$) between the paramag-

netic 3d Fe³⁺ moment ($g\mu_B S_d$) (g is the Landé factor and μ_B is the Bohr magneton) and the conduction π -electrons in the BETS molecule (π –d interaction)^{1,6} generates a large magnetic field ($\mathbf{B}_{\pi d}$) that cancels most of the externally applied magnetic field (\mathbf{B}_0) when the latter is large ($B_0 \sim 17 - 45 \text{ T}$) and aligned parallel to the *ac* plane. This suggests that the $\mathbf{B}_{\pi d}$ ($B_{\pi d} = J_{\pi d} \langle S_d \rangle / g\mu_B$, where $\langle S_d \rangle$ is the average value of the Fe³⁺ spin polarization.) at the conducting π -electrons is on the order of 30 T and its direction is antiparallel to \mathbf{B}_0 . It has also been proposed that the Larkin-Ovchinkov-Fulde-Farrell (LOFF) phase is present near the boundary of the FISC phase.^{12,13}

The magnetic PM–AFI phase transition, which occurs at $B_0 < 11 \text{ T}$ (Néel temperature T_N), coincides with a metal-insulator (MI) transition^{1,14,15} (transition temperature T_{MI}). The property $T_N = T_{MI}$ indicates that the MI and AFI transitions are cooperative transitions.^{1,14,15} Thus, it is expected this PM–AFI transition is also a result of the π –d interaction, since the study of its iso-structural nonmagnetic and non-3d-electron analog λ -(BETS)₂GaCl₄ shows that it exhibits a behavior^{7,16} that is completely different from that of λ -(BETS)₂FeCl₄. However, the detailed role of the π –d interaction for the PM–AFI phase transition is not yet clear because it has not yet been revealed by direct experimental evidence.

In this paper, measurements of the proton nuclear magnetic resonance (NMR) spectrum are reported for a small ($\sim 4 \mu\text{g}$) single crystal of λ -(BETS)₂FeCl₄ in a magnetic field $\mathbf{B}_0 = 9 \text{ T}$ aligned parallel to the *a*-axis in the *ac*-plane over a temperature range 2.0–180 K. These measurements probe the distribution and the origin of

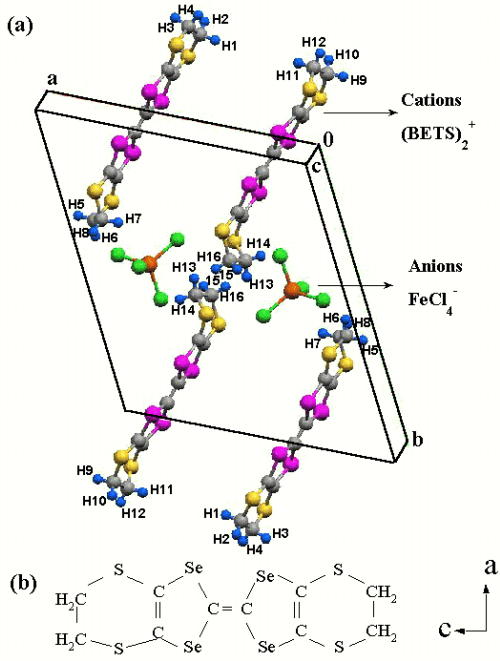


FIG. 1: (color online) (a) The crystal structure of λ -(BETS)₂FeCl₄ with all 32 hydrogen atoms labeled in a unit cell. Atoms in color: Red –Fe; Green –Cl; Blue –H; Grey –C; Yellow –S; Pink –Se. (b) The BETS molecule.

the static local magnetic field at the proton sites in the PM and AFI states as well as across the PM–AFI phase transition. The observed properties should help to establish a microscopic model for the PM–AFI phase transition.

One important result of this investigation is that the dominant local magnetic field at the proton sites comes from the large dipolar field of the 3d Fe³⁺ ion moments. A mean field model based on the dipolar field of the Fe³⁺ moments is used to calculate the proton NMR spectrum and provides a good fit to the measured spectra. Besides this, the total exchange constant J_0 between an Fe³⁺ ion and its two nearest neighbors is determined to be $J_0 \sim -1.7$ K from a fit to the spectrum data. These measurements also show that there is a significant change in the static local magnetic field distribution at the proton sites across the PM–AFI phase transition.

The rest of this paper is organized as follows. Section II presents the experimental details and Section III has the experimental results for the proton NMR spectra, including frequency distributions, shifts, and linewidths. Section IV presents the model for the spectrum, along with the comparison with the measured spectra. The conclusions are stated in Section V.

II. EXPERIMENTAL DETAILS

The needle-like single crystal λ -(BETS)₂FeCl₄ samples were prepared as described by Montgomery et al with a standard electrochemical oxidation method.¹⁷ The dimensions of the sample used for these ¹H-NMR measurements are (1.2 ± 0.1) mm \times (0.065 ± 0.010) mm \times (0.018 ± 0.005) mm, which corresponds to (3.8 ± 1.8) μ g in mass and $(2.7 \pm 1.3) \times 10^{16}$ protons.

The NMR coil used was 40 turns of 0.025 mm diameter bare copper wire wound on a 0.075 mm diameter wire form. The coil was held to the rest of the probe circuit by two 125 μ m diameter Cu wire leads with Teflon insulation, which was removed close to the ends where the coil was soldered to them. Commercial pure acetone was used for cleaning the coil and its surroundings when the NMR coil was set on the probe to reduce the spurious proton signals relative to the signals from such a small sample. Finally, a single needle-like λ -(BETS)₂FeCl₄ single crystal sample was slid into the coil, carefully aligned close to $B_0 \parallel a$ in the *ac*-plane, and held in place with a very small amount of commercial Apiezon grease on each end. The orientation uncertainty is estimated to be $\sim \pm 5^\circ$.

As shown in a preliminary report,¹⁸ the spurious proton signal was estimated to be less than $\sim 4\%$ of the signal from the λ -(BETS)₂FeCl₄ sample by comparing the signal with and without the sample in the coil. Thus, in these measurements the spurious proton signal has an insignificant size.

The ¹H-NMR frequency-swept spectra were obtained using standard spin-echo techniques carried out with a spectrometer and probe built at UCLA. Since the proton has a gyromagnetic ratio $\gamma_I = 42.5759$ MHz/T, the frequency ν for the excitation pulses used for the spectrometer is near $\nu \sim \nu_0 = \gamma_I B_0 = 382.6935$ (MHz), where ν_0 is the proton Larmor frequency in the external field. The value of B_0 used in this experiment was $B_0 = 8.9885$ T (for simplicity, often referred to here as 9 T).

Because the NMR spectrum covers a wide range in frequency up to 14 MHz (3.3 kG), short rf pulses and a wide receiver bandwidth (± 1 MHz) were used to record the spin-echo signals. The pulse sequence that optimized the height of the spin echo used to record the NMR signal was a 0.2 μ s $\pi/2$ pulse ($B_1 = 294$ G, 1.25 MHz proton frequency) followed by a 0.3 μ s pulse separated by a time interval τ ($\tau \sim 5$ μ s) for most of the measurements. For a viable signal-to-noise ratio, each echo signal was averaged 2000 times at 180 K and 128 times at 4.2 K and lower temperatures. The uncertainty associated with the signal-to-noise ratio is probably the main source of error in the data. The uncertainties include $\sim \pm 1\%$ in T and $\pm 5^\circ$ in the field alignment.

At low T , the spectrum is very wide (~ 12 MHz) and the frequency sweep covered a range as high as 370 to 400 MHz and used a typical frequency step for each acquisition of 0.2 – 0.5 MHz. When a wide frequency sweep range was used, the probe circuit was retuned every 4

MHz to maintain a uniformly high sensitivity (above 85%) for recording the proton spectrum. The spectra were analyzed with frequency-shifted and -summed Fourier transform processing.¹⁹

III. RESULTS

A. $^1\text{H-NMR}$ spectra

Figure 2 shows the normalized $^1\text{H-NMR}$ absorption spectra $[\chi''(\nu)]$ of a λ -(BETS)₂FeCl₄ single crystal as a function of the frequency ν shifted from the Larmor frequency ν_0 with an applied magnetic field of 8.9885 T parallel to the a -axis in the ac -plane over the temperature range 180 K to 2 K.

Over most of the temperature range, the spectra have six main peaks which can be divided into two groups (low frequency side and high frequency side) with 3 main peaks for each. As the temperature T is lowered from 180 to 4.2 K in the PM state, the spectrum broadens significantly, its center shifts to lower frequency and the splitting between the peaks increases. For such a complex spectrum, a reasonable measure of its center is the first moment, $\langle \nu \rangle$, given by²⁰

$$\langle \nu \rangle = \frac{\sum_i \nu_i \chi''_i(\nu_i)}{\sum_i \chi''_i(\nu_i)}, \quad (1)$$

where i indexes equally spaced frequency steps. The average shift of the spectrum indicated by the dashed line in Fig. 2, is then $\Delta\nu = \langle \nu \rangle - \nu_0$. Also, some additional weak structures gradually develop at lower T . As the sample is cooled further into the AFI phase ($T \leq T_{MI} = 3.5$ K), the details of the spectrum become somewhat smeared, an additional peak at 4.25 MHz appears and it grows larger with further cooling (solid line in Fig. 2).

As discussed in later sections, this relatively complex spectrum is caused mainly by the dipolar field of the 3d Fe³⁺ ion electron spin moments ($S_d = 5/2$, $g \approx 2$) at 16 magnetically inequivalent proton sites in both the PM and AFI phases. In both phases, these moments are present, the major differences being that they should have long-range order and a different orientation in the AFI state.

The changes of the spectrum vs temperature below T_{MI} , such as the smearing of the spectrum details and the growth of the new peak at the high frequency side, occur gradually rather than suddenly. This behavior indicates a continuous change of the local magnetic field distribution at the proton sites as T is lowered. Its origin is probably the development of the canted-antiferromagnetic phase as observed from the field dependence of magnetization and capacitance measurements reported for λ -(BETS)₂FeCl₄.^{2,5}

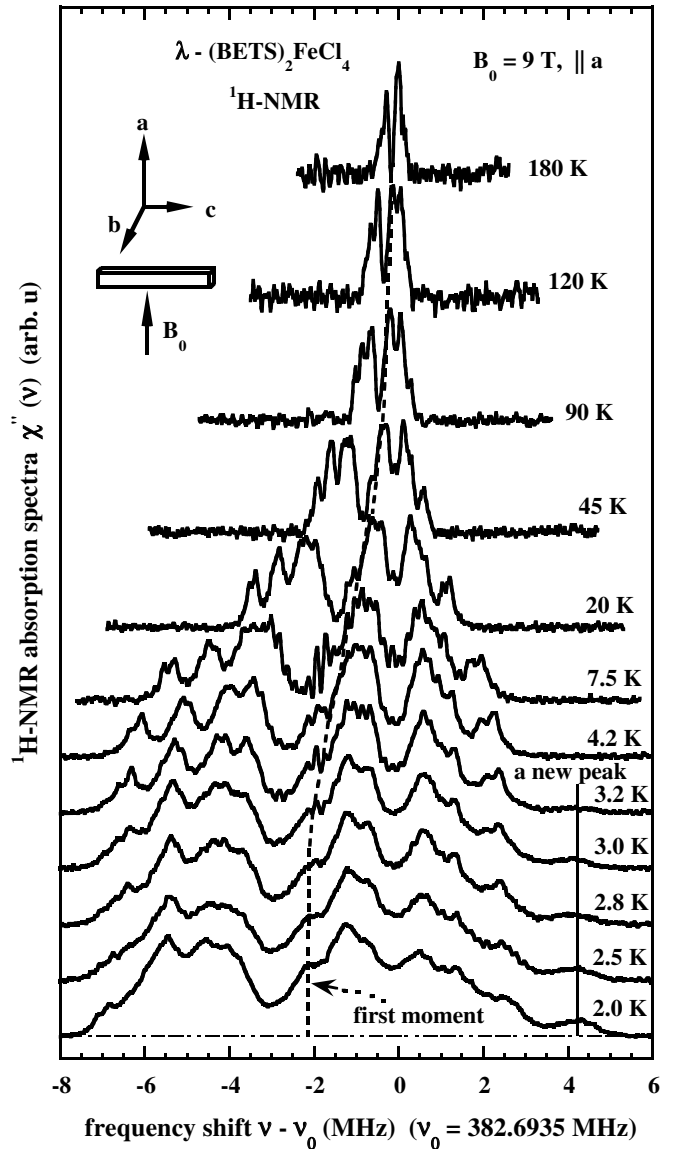


FIG. 2: Normalized $^1\text{H-NMR}$ absorption spectra of a single crystal of λ -(BETS)₂FeCl₄ as a function of the frequency shift from the proton Larmor frequency $\nu_0 = 382.6935$ MHz from 180 K to 2 K with an applied magnetic field of 8.9885 T parallel to the a -axis in the ac -plane. The solid vertical line at $\nu - \nu_0 = 4.25$ MHz indicates a new peak below $T \leq T_{MI} = 3.5$ K, and the dashed line through the spectra shows the first moment (in frequency) for each of the spectra.

B. $^1\text{H-NMR}$ frequency shift

Figure 3 shows the $^1\text{H-NMR}$ frequency shift $\Delta\nu$ as a function of T , and the inset of Fig. 3 plots $1/|\Delta\nu|$ vs T . A clear discontinuity of $\Delta\nu$ at $T = T_{MI}$ is seen. The error bars are our best estimate of the uncertainty in our data analysis.

The NMR frequency is given by the magnitude of the

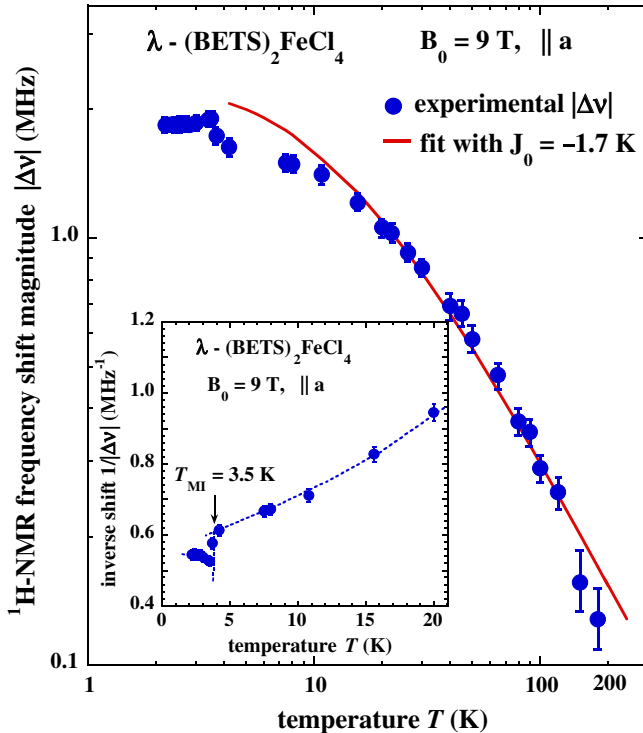


FIG. 3: (color online). T –dependence of the ^1H -NMR frequency shift $\Delta\nu$ for a single crystal of λ -(BETS) $_2\text{FeCl}_4$ from 180 K to 2 K with $\mathbf{B}_0 = 8.9885$ T parallel to the a -axis in the ac -plane. The solid line is a fit to Eqs. (6)–(10) with $J_0 = -1.7$ K. The inset shows the discontinuity of $1/|\Delta\nu|$ vs T across the PM–AFI phase transition at 3.5 K. The dashed line is a guide to the eye.

total magnetic field at the nucleus. Since it is the sum of the large external \mathbf{B}_0 plus the much smaller field generated by the sample ($\Delta\mathbf{B}_0$), it is easily shown that the field shift caused by the magnetic properties of the sample is the component of its field parallel to \mathbf{B}_0 ($\Delta B_{||}$). The values of $\Delta\nu$ in Fig. 3 represent the average of $\Delta B_{||}$ over the proton sites ($\langle \Delta B_{||} \rangle$) with

$$\Delta\nu = \gamma_I \langle \Delta B_{||} \rangle. \quad (2)$$

Thus, the origin of $\Delta\nu$ is the distribution of $\Delta B_{||}$ over the proton sites.

At 180 K, $\Delta\nu$ has a value of $-(0.13 \pm 0.02)$ MHz, while at 4 K it reaches $-(1.750 \pm 0.005)$ MHz. Below $T_{MI} = 3.5$ K, $\Delta\nu$ has a rather weak temperature dependence, as shown in the inset of Fig. 3. The sudden decrease of $1/|\Delta\nu|$ at T_{MI} indicates an increase of the average static local magnetic field at the proton sites due to the PM–AFI phase transition. Its sharpness is evidence that the PM–AFI phase transition is first order.

The negative sign of $\Delta\nu$ indicates that the direction of the average static local magnetic field is opposite to the external magnetic field. But this does not mean that the average static moment is negative. The negative sign is

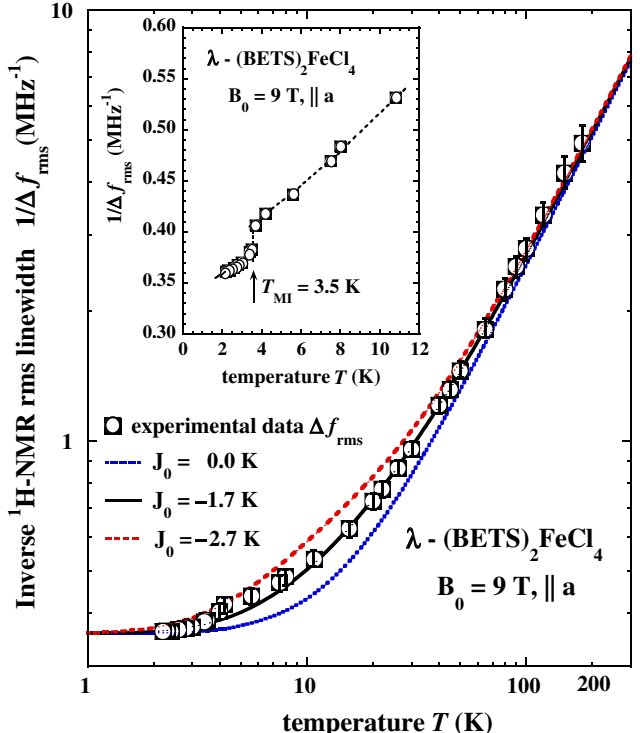


FIG. 4: (color online). T –dependence of $1/\Delta f_{\text{rms}}$ for a single crystal of λ -(BETS) $_2\text{FeCl}_4$ from 180 K to 2 K with $\mathbf{B}_0 = 8.9885$ T parallel to the a -axis in the ac -plane. The black solid line shows the best fit to the data from Eqs. (6)–(10) with $J_0 = -1.7$ K. The inset shows the low T data across the PM–AFI phase transition, with a dashed line as a guide to the eye.

determined by the proton positions relative to the Fe^{3+} ions in the crystal lattice.

C. ^1H -NMR spectrum linewidth

A reasonable quantitative measure of the local field distribution that generates the proton spectrum of λ -(BETS) $_2\text{FeCl}_4$ is the root mean square (rms) linewidth, Δf_{rms} , i.e. the square root of the second moment, $\langle \Delta\nu^2 \rangle^{1/2}$, given by^{20,21}

$$\Delta f_{\text{rms}} \equiv \langle \Delta\nu^2 \rangle^{1/2} = \left[\frac{\sum_i (\nu_i - \langle \nu \rangle)^2 \chi''(\nu_i)}{\sum_i \chi''(\nu_i)} \right]^{1/2}. \quad (3)$$

The measurements of Δf_{rms} for protons as a function of T in λ -(BETS) $_2\text{FeCl}_4$ are shown in Fig. 4, where $1/\Delta f_{\text{rms}}$ is plotted as a function of T . At 180 K, Δf_{rms} has the value of (0.205 ± 0.005) MHz and it reaches (2.50 ± 0.10) MHz at $T_{MI} = 3.5$ K. The error bar is estimated to be equal to or smaller than the size of the marker below ~ 50 K.

Across $T_{MI} = 3.5$ K, as for $\Delta\nu$ in Fig. 3, there is a sudden increase of Δf_{rms} in Fig. 4 that also indicates a first order phase transition.

There are several important properties of the data shown in Figs. 2–4. At $T > 50$ K, it can be shown that the T –dependence of all of them ($\langle \nu \rangle$, $\Delta\nu$ and Δf_{rms}) follows the Curie–Weiss relation with a Curie–Weiss temperature $\Theta \simeq 5.5$ K. They also follow the Brillouin function [$B_J(x)$] behavior using the parameters for the Fe^{3+} spins. This result is a strong indication that the dominant contribution to $\Delta\mathbf{B}_0$ is the dipolar field at the proton sites from the magnetization of the Fe^{3+} spins.

An important issue for characterizing the data is that they extend well into the low T regime; i.e., at 9 T, the Zeeman splitting between the highest and lowest Fe^{3+} spin states is $5 \times g\mu_B B_0/k_B \simeq 60.5$ K, where k_B is the Boltzmann constant. For this reason, instead of the more commonly used Curie–Weiss law, which is a high T approximation ($T \gg g\mu_B S_d/k_B \approx 30.2$ K), we characterize the data with the Brillouin function, which includes magnetic saturation at low T . Also, since there is a significant total antiferromagnetic (negative) exchange interaction J_0 among the Fe^{3+} moments,^{5,22} the Brillouin function used here is modified to include a simple, approximate mean field correction.

For non-interacting moments, the magnetization [$M(x_0)$] is given by²³

$$M(x_0) = N_A g\mu_B J B_J(x_0), \quad (4)$$

where N_A is Avogadro's number, $J = S_d = 5/2$ for the Fe^{3+} , and $B_J(x_0)$ is

$$B_J(x_0) = \frac{2J+1}{2J} \coth\left(\frac{2J+1}{2J}x_0\right) - \frac{1}{2J} \coth\left(\frac{1}{2J}x_0\right), \quad (5)$$

where

$$x_0 = \frac{Jg\mu_B B_0}{k_B T}. \quad (6)$$

The effect of J_0 for an antiferromagnetic exchange interaction between the nearest neighbor Fe^{3+} moments can be modeled as an additional magnetic field component (B') antiparallel to \mathbf{B}_0 ,²³ given by

$$B' = \frac{|J_0|Jk_B}{g\mu_B} B_J(x) \approx \frac{|J_0|Jk_B}{g\mu_B} B_J(x_0), \quad (7)$$

where

$$x = x_0 + x' = \frac{Jg\mu_B(B_0 - B')}{k_B T}, \quad (8)$$

and the right side of Eq. 7 has been used for B' . Because the value obtained later for B' is substantially smaller than B_0 , this approximation is a reasonable one. Thus, the mean field modified Brillouin function used to model

our data is $B_{JM}(x)$ and the corresponding formula to fit Δf_{rms} is

$$\Delta f_{\text{rms}} = C' M(x) = C' N_A g\mu_B J B_{JM}(x), \quad (9)$$

where

$$B_{JM}(x) = B_J(x_0 + x'), \quad (10)$$

and C' and J_0 are adjusted to give the best fit to the data.

As shown in Fig. 4, from the T –dependence of Δf_{rms} the best fit is obtained with $J_0 = -(1.7 \pm 0.2)$ K. This corresponds to a maximum total exchange field of ~ -3 T below ~ 5 K. The negative sign of J_0 indicates that the Fe^{3+} ions have an antiferromagnetic (AFM) exchange interactions with their nearest neighbors. Since each Fe^{3+} ion has two nearest neighbors³ (actually three closest ones: two are at ~ 6.6 Å away, and one at ~ 7.6 Å away) the exchange constant J_{dd} between each pair of Fe^{3+} ions is, $J_{dd} \approx J_0/2 = -(0.85 \pm 0.10)$ K, which agrees with theoretical expectations (~ -0.64 K).²² The parameter C' has a fitted value of (100 ± 6) mol.Fe–Hz/emu. The overall difference between the fit and the Δf_{rms} data is below $\sim 5\%$, except near the phase transition, where it has $\sim 10\%$.

Similarly, the frequency shift $\Delta\nu$ (Fig. 3) can also be well-fitted with Eqs. (6)–(10) from 180 K down to 10 K with the same fit value of J_0 . But its deviation is slightly larger below ~ 10 K. This is possibly caused by not including the demagnetization and Lorentz fields to the local field B' in Eq. (7) for the shift.

The property that $\Delta f_{\text{rms}} > |\Delta\nu|$ shows that there is a broad static local magnetic field distribution in λ -(BETS)₂FeCl₄. It occurs because there are 16 inequivalent ¹H-sites at which the dipolar field from the Fe^{3+} moments has a large variation.

As discussed in more detail below, these proton shift properties support the conclusion that they are dominated by the dipolar field from the 3d Fe^{3+} ion electron moments. The sudden change in the spectrum at $T_{MI} = 3.5$ K, as well as seen from those proton shift properties, reflects a comprehensive change of the static local magnetic field distribution at the ¹H-sites due to the AF ordering of the Fe^{3+} electron spins.

IV. DISCUSSION

In this section, the local magnetic fields at the proton sites and the ¹H-NMR spectrum are calculated, and the nature of the AFI phase transition is discussed.

A. Model for the ¹H-NMR spectra

Generally NMR spectra are determined by the values of static local magnetic field and the distribution of the

local magnetic field at the nucleus sites in the studied material. Here, a model for the spectrum is presented and applied to λ -(BETS)₂FeCl₄. It considers all possible major sources which include the dipolar field of the Fe³⁺, the exchange interactions with the Fe³⁺ ion and π -electrons, the dipolar field of the neighboring proton nuclei, and the demagnetization and Lorentz contributions^{20,21,22,24} to the local field at the proton sites.

In λ -(BETS)₂FeCl₄ single crystals,³ there are 16 inequivalent proton sites per unit cell (see Fig. 1). Thus, up to 16 different lines in ¹H-NMR spectrum can be expected. Each of these 16 protons will have, in general, a different shift in the NMR frequency depending on its position in the crystal lattice.

The Hamiltonian H_I of the system for the ¹H-NMR can be described as²⁰

$$H_I = H_{IZ} + H_{II} + H_{Id}^{\text{dip}} + H_{Id}^{\text{hf}} + H_{I\pi} + H^{\text{dem}} + H^{\text{Lor}}, \quad (11)$$

where H_{IZ} is the Zeeman Hamiltonian of the proton nuclei in the external field B_0 , H_{II} is the proton-proton nuclear dipolar interaction Hamiltonian, H_{Id}^{dip} and H_{Id}^{hf} are the dipolar coupling and transferred hyperfine coupling from the 3d Fe³⁺ electrons to the protons, respectively, $H_{I\pi}$ is the hyperfine coupling of the proton nucleus to the BETS π -electrons, and the last two terms, H^{dem} and H^{Lor} , are the bulk demagnetization and Lorentz contributions, respectively.^{20,25} All of these terms contribute to the static local magnetic field at the proton sites and all but the first cause the ¹H-NMR frequency shifts.

Since the hyperfine couplings are proportional to Z^2 , where Z is the atomic number for the corresponding nucleus (for protons, $Z = 1$),²⁰ the proton hyperfine couplings to the π -electrons ($H_{I\pi}$) and to the Fe³⁺ electrons (H_{Id}^{hf}) are expected to be negligible. Thus, the system Hamiltonian can be rewritten as

$$H_I \approx H_{IZ} + H_{II} + H_{Id}^{\text{dip}} + H^{\text{dem}} + H^{\text{Lor}}. \quad (12)$$

Among these terms it is expected that the dipolar field of the Fe³⁺ ion electron spins, i.e. the contribution of Hamiltonian H_{Id}^{dip} , to be the dominant source contributing to the static local magnetic field at the proton sites, as seen from the analysis in the following sections.

Note that any interactions, both direct and indirect, between the π electrons and the Fe³⁺ ions (π -d interaction) or between the Fe³⁺ ions (d-d interaction) will affect the polarization of the Fe³⁺ electron moments, thereby modifying the dipolar field from the 3d Fe³⁺ ions at the proton sites. In what follows, the effects of these interactions are considered, and the total d-d exchange interactions including those through the Cl⁻²² and the conduction π -electrons (RKKY interaction) are included in the calculation with mean field approximation using the modified Brillouin function. But the direct π -d interaction is considered to be small because the magnetization of the conduction π -electrons is very small comparing with that of the Fe³⁺, thus it will not be included. Some discussions will be presented later.

The dipole moment $\vec{\mu}_j$ of the Fe³⁺ ion j produces a magnetic field \vec{B}_{ij} at the proton site i given by²⁶

$$\vec{B}_{ij} = \frac{3 \vec{r}_{ij} (\vec{\mu} \cdot \vec{r}_{ij})}{\vec{r}_{ij}^5} - \frac{\vec{\mu}_j}{\vec{r}_{ij}^3}, \quad (13)$$

where \vec{r}_{ij} is the position vector from the proton site i to the Fe³⁺ ion site j .

Thus, the total dipolar field $\langle \vec{B}_i \rangle$ at the proton site i is

$$\langle \vec{B}_i \rangle = \sum_j \langle \vec{B}_{ij} \rangle, \quad (14)$$

$$= \sum_j \left\langle \left[\frac{3 \vec{r}_{ij} (\vec{\mu} \cdot \vec{r}_{ij})}{\vec{r}_{ij}^5} - \frac{\vec{\mu}_j}{\vec{r}_{ij}^3} \right] \right\rangle, \quad (15)$$

and the magnetization $\vec{M}(x)$ of the Fe³⁺ moments is

$$\vec{M}(x) = \frac{\sum_j \langle \vec{\mu}_j \rangle}{V}. \quad (16)$$

By considering Eqs. (6)–(10) and (13)–(16), and assuming that the magnetization $\vec{M}(x)$ has the same direction as \mathbf{B}_0 , one obtains

$$\langle \vec{B}_i \rangle \approx \frac{g\mu_B J B_{JM}(x)}{B_0} \sum_{j=-N}^{+N} \left[\frac{3\vec{r}_{ij}(\vec{B}_0 \cdot \vec{r}_{ij})}{\vec{r}_{ij}^5} - \frac{\vec{B}_0}{\vec{r}_{ij}^3} \right], \quad (17)$$

where $i = 1, 2, \dots, 16$, which indexes the proton sites, and x is a T -dependent variable as defined by Eqs. (6)–(8).

Equation (17) is used to calculate the local field at all T in the PM phase. The mean field approximation for the Fe³⁺ exchange interactions is included in $B_J(x)$.

At high T ($g\mu_B B_0 J \ll k_B T$), Eq. (17) can also be written as

$$\langle \vec{B}_i \rangle \approx \frac{(g\mu_B)^2}{3k_B} \frac{J(J+1)}{T + \Theta} \sum_{j=-N}^{+N} \left[\frac{3\vec{r}_{ij}(\vec{B}_0 \cdot \vec{r}_{ij})}{\vec{r}_{ij}^5} - \frac{\vec{B}_0}{\vec{r}_{ij}^3} \right], \quad (18)$$

where Θ is the Curie-Weiss temperature.

The field \mathbf{B}_0 can be expressed as $\mathbf{B}_0 = B_0(\sin \theta \cos \phi \hat{i} + \sin \theta \sin \phi \hat{j} + \cos \theta \hat{k})$, where θ and ϕ are standard spherical coordinates in the Cartesian system,²⁷ and the dipolar field components $\langle B_i \rangle_x$, $\langle B_i \rangle_y$, and $\langle B_i \rangle_z$ along x, y, z directions, respectively, can be calculated for each of the 16 inequivalent proton sites with Eq. (17) by considering the coordinates of all the inequivalent proton sites and the Fe³⁺ ion positions.

Since the values of $\langle \vec{B}_i \rangle$ obtained in the next section obey $|\langle \vec{B}_i \rangle| \ll B_0$, the contribution of $\langle \vec{B}_i \rangle$ to the shift of the proton spectrum comes only from the component of $\langle \vec{B}_i \rangle \parallel \mathbf{B}_0$ ($B_{\parallel}^{\text{dip}}$).

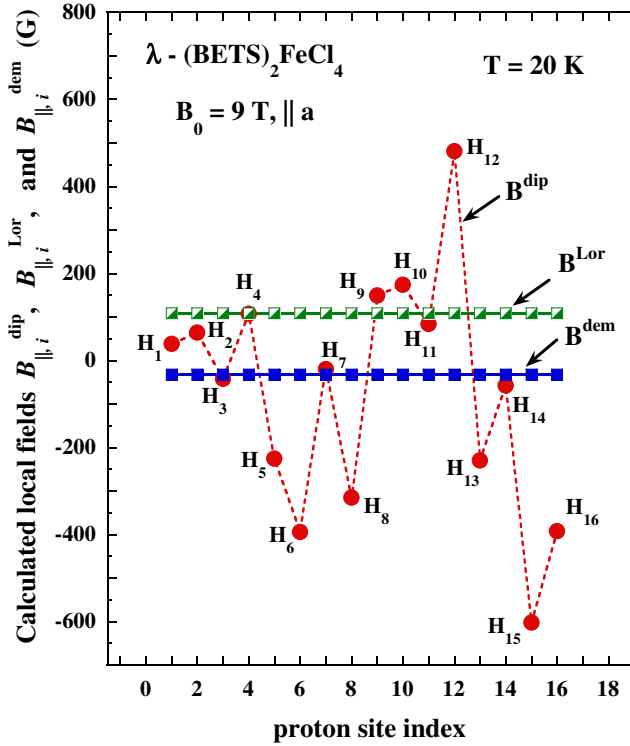


FIG. 5: (color online). Calculated dipolar ($B_{\parallel i}^{\text{dip}}$), Lorentz ($B_{\parallel i}^{\text{Lor}}$), and demagnetization field ($B_{\parallel i}^{\text{dem}}$) components parallel to \mathbf{B}_0 at each of the 16 inequivalent proton sites (index i) in a single crystal of λ -(BETS)₂FeCl₄ at 20 K. The alignment of $\mathbf{B}_0 = 8.9885$ T is parallel to the a -axis in the ac -plane. The solid and dashed lines are guides to the eye.

B. Calculated local magnetic field at the proton sites

Figure 5 shows the calculated component of the Fe³⁺ ion dipolar field parallel to \mathbf{B}_0 at the 16 inequivalent proton sites H1, H2, ..., H16 in the crystal lattice using Eq. (17) at $T = 20$ K and $B_0 = 8.9885$ T. The number of unit cells included is $(2 \times 100 + 1)^3$; i.e., $N = 100$. The crystal ac -plane is chosen to be in the xz -plane with considerations from the lattice triclinic to Cartesian system.

The values of the components of the Lorentz field, $B_{\parallel i}^{\text{Lor}}$, and the demagnetization field, $B_{\parallel i}^{\text{dem}}$, parallel to \mathbf{B}_0 , based on the shape of the needle-shape single crystal sample and the magnetization $M(x)$ [Eqs. (5)–(10)], are +108.3 G and -32.5 G, respectively,^{25,28} as shown in Fig. 5. The net shift from both of these contributions is their sum, i.e. +75.8 G, which is small, but not completely negligible. The small spacial variations²⁵ of the demagnetization field across the sample have been neglected.

Also, the calculated contribution of H_{II} is only ≤ 3 G among the 16 inequivalent proton sites, as confirmed by

the spin-echo decay measurements.²⁹ Since it is so small, it is also neglected here.

Thus, $B_{\parallel i}^{\text{dip}}$ obtained from Eq. (17) (see Fig. 5) is the dominant contribution to the structure of $\chi''(\nu)$. Since $B_{\parallel i}^{\text{Lor}}$ and $B_{\parallel i}^{\text{dem}}$ are nearly constant over all the proton sites, they have a negligible effect on the structure of $\chi''(\nu)$; their contribution constitutes a shift in frequency or field but with almost the same amount for each proton sites ($\sim 25\%$ to the average $\Delta\nu$ at 20 K).

The values of $B_{\parallel i}^{\text{dip}}$ at 20 K cover a wide range of field, from ± 20 G up to ± 600 G, depending on the proton positions in the crystal lattice. For example, at the proton site H15 it is ~ -600 G, and $\sim +500$ G at the proton site H12. The positions of these proton sites are all labeled in Fig. 1. The proton site (H15) that has the largest $B_{\parallel i}^{\text{dip}}$ from the Fe³⁺ ions is that which is closest to the nearby Fe³⁺ ion plane in the crystal lattice. The range of field (~ -600 – +600 G) that $B_{\parallel i}^{\text{dip}}$ covers corresponds to a range of frequency of ~ 5 MHz.

C. Calculated ¹H-NMR spectra from the dipolar field contributions

In this section the model for the proton absorption spectrum [$\chi''_{\text{mod}}(\nu)$] is calculated. The first step is to calculate the static local magnetic field $B_{\parallel i}^{\text{dip}}$ at each of the 16 inequivalent proton sites, as described in Sections IV A and B. The second step is to convolve this field distribution with a set of Gaussian functions, y_i , each of which has a maximum amplitude of 1 and the same width δ at each proton site i .²¹ In this case,

$$\chi''_{\text{mod}}(\nu) = \sum_{i=1}^{16} \exp \left[-\frac{(\nu - \gamma_0 B_{\parallel i}^{\text{dip}})^2}{2\delta^2} \right]. \quad (19)$$

Plots of $\chi''_{\text{mod}}(\nu)$, calculated with this model and the value of $\delta = 0.15$ MHz, are shown in Fig. 6 for $T = 20$ K with $B_0 = 8.9885$ T aligned close to the a -axis ($\theta = 90^\circ \pm 5^\circ$) and near the ac -plane ($\phi = -15^\circ$ – +20°). These angles are selected because they are close to what is needed for comparison with the measurements. As can be seen in Fig. 6, $\chi''_{\text{mod}}(\nu)$ is fairly sensitive to θ and ϕ which are determined by the direction of \mathbf{B}_0 .

D. Comparison of the model to the measured spectra

Figure 7 shows the calculated $\chi''_{\text{mod}}(\nu)$ (upper) using $B_0 = 8.9885$ T with $\theta = +85^\circ$ and $\phi = +5^\circ$, and the measured $\chi''(\nu)$ (lower) at 20 K, for comparison. The frequency $\nu_0 = 382.6935$ MHz. Here, the calculated result includes the dipolar field from the Fe³⁺ electrons, and corrections for the Lorentz and bulk demagnetization fields; i.e., the calculated spectrum comes from the

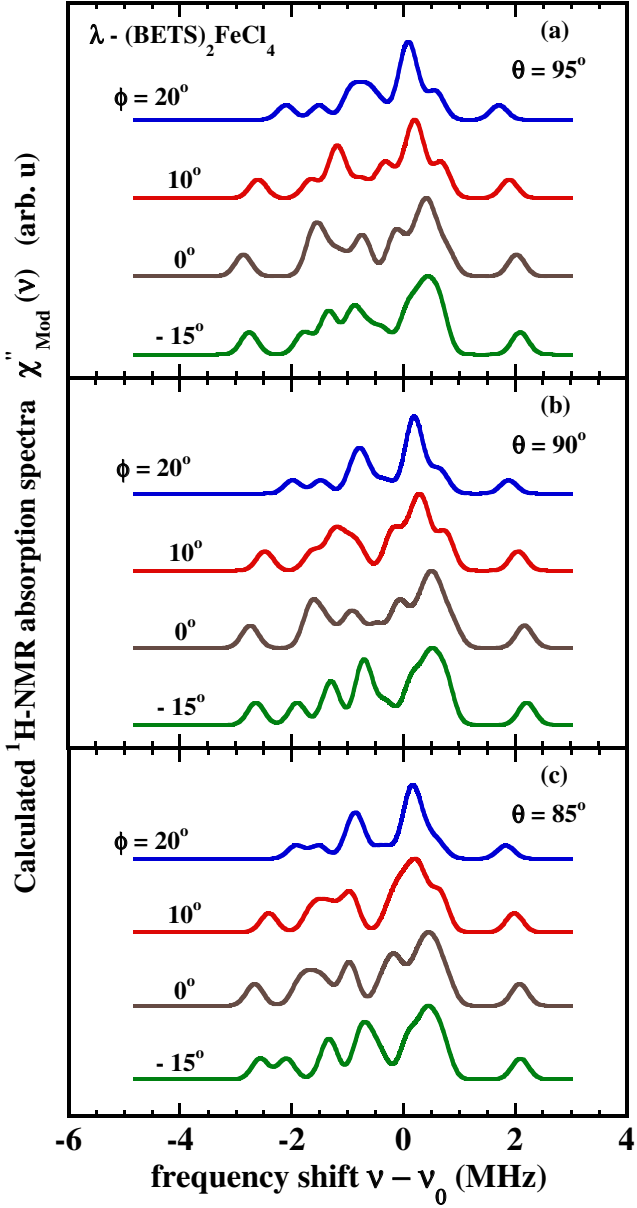


FIG. 6: (color online). Calculated proton $\chi''_{\text{mod}}(\nu)$ from the 3d Fe^{3+} ion electron dipolar contributions in single crystal λ -(BETS)₂FeCl₄ at 20 K with $\mathbf{B}_0 = 8.9885$ T aligned close to the a -axis ($\theta = 90^\circ \pm 5^\circ$) and near the ac -plane ($\phi = -15^\circ - +20^\circ$). The Larmor frequency $\nu_0 = 382.6935$ MHz.

dipolar field of the Fe^{3+} electrons shifted by the Lorentz and bulk demagnetization fields.

There are several small differences between the measured and calculated model spectra shown in Fig. 7. One is that at 20 K, the shift in the center of the spectrum differs by ~ 42 kHz (~ 100 G). This is quite small compared to the separation of the outer peaks, which is 4.65 MHz (1.09 kG) for both the measured and calculated spectra. On the other hand, $\Delta f_{\text{rms}} = 1.126$ MHz and 1.387 MHz

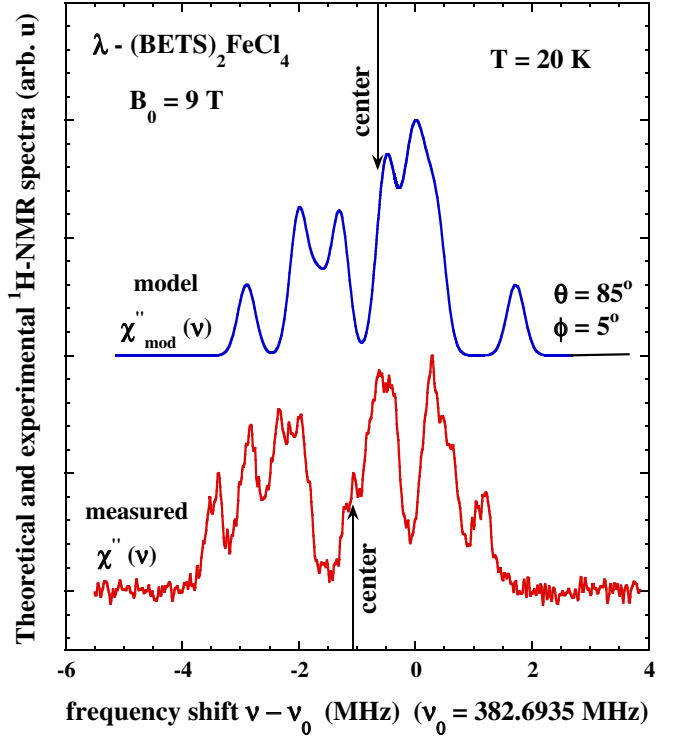


FIG. 7: (color online). Comparison of the calculated $\chi''_{\text{mod}}(\nu)$ (upper) with the measured $^1\text{H-NMR}$ absorption spectrum $\chi''(\nu)$ (lower) in a single crystal of λ -(BETS)₂FeCl₄ at 20 K. For $\chi''_{\text{mod}}(\nu)$, the value of \mathbf{B}_0 is 8.9885 T aligned with $\theta = +85^\circ$ and $\phi = +5^\circ$, which is close to the a -axis and near the ac -plane. The vertical arrows indicate the center (first moment) of each line.

for the model and measured values, respectively, which corresponds to a difference of $\sim 18\%$. Another small difference is in the shape of the spectra. These similarities in the model and measured spectra strongly support for the conclusion that the proton spectrum in λ -(BETS)₂FeCl₄ is dominated by the dipole field of the Fe^{3+} ions.

An important question is what is responsible for the small difference between the spectra calculated with the model that has been used and the measured spectra. It is probably caused by not including all the details of the exchange interactions (including the d-d exchange interactions through the Cl^- and through the BETS conduction π -electrons) in which the Fe^{3+} electron spins participate when using the mean field $M(x)$ or $B_{JM}(x)$ to model the polarization of the Fe^{3+} electron spins.

Also, an important aspect of the π -d interaction which is also part of the d-d exchange interactions is that it should be responsible for the coordination of the occurrence of the PM-AFI phase transition.

It is expected that if all of the exchange interactions are included in detail, they will cause a small change in the moment of the Fe^{3+} ions and their polarization will not be precisely along \mathbf{B}_0 , even in the PM phase. It

is likely that these additional factors are responsible for the relatively small difference between the measured and calculated shift and width in the ^1H -NMR spectrum. To include them in a model is beyond the scope of this paper.

E. The local magnetic field in the AFI state and the nature of the PM–AFI phase transition

As in the PM state, the local magnetic field at the proton sites in the AFI state ($T \leq T_{MI} = 3.5$ K) is also dominated by the dipolar field from the Fe^{3+} ions, even though Eq. (17) is not specific to and may not apply in the AFI state. In both phases, the Fe^{3+} ion electron spin moments are present and the general Hamiltonian H_I of the ^1H -NMR system Eq. (11) or (12) applies in both the PM and AFI states.

However, the change of the ^1H -NMR spectra in λ -(BETS)₂FeCl₄ is significant. On cooling from the PM to the AFI state, the spectrum broadens, the splittings are smeared out, and a new peak appears on the high frequency side.

It is unlikely that these changes are caused by variations in the Lorentz or demagnetization field because the contribution from each of them is essentially the same at each proton site, even though they are proportional to the Fe^{3+} ion electron susceptibility.

Therefore the changes of the details in the proton spectra at any T (including in the PM and AFI phases) come mainly from the change of the dipolar field of the 3d Fe^{3+} ions, which in part are changed by the effect of π -d and d-d interactions on the polarization of the Fe^{3+} moments. The major difference for the Fe^{3+} moments is that they should have long-range order in the AFI state, which is formed by the π -d and d-d interactions.^{1,14,15}

The evidence from the change of the ^1H -NMR spectra, as well as that reflected by the discontinuities of the frequency shift $\Delta\nu$ and the rms linewidth Δf_{rms} , is indicative of a first order nature for the PM–AFI phase transition in λ -(BETS)₂FeCl₄.^{22,30}

V. CONCLUSIONS

^1H -NMR spectrum measurements are reported for a single crystal of the organic conductor λ -(BETS)₂FeCl₄,

using an applied magnetic field $B_0 = 8.9885$ T parallel to the a -axis in the ac -plane over the temperature range 2.0–180 K. They provide the distribution of the static local magnetic field at the proton sites in both the PM and the AFI phases.

The experimental spectra have six main peaks and become progressively broadened and shifted as T is decreased from 180 K to ~ 5 K. For $T \leq T_{MI} = 3.5$ K (below the PM–AFI transition), an extra peak appears on the high frequency side, the details of the spectrum become smeared, and changes in the frequency shift and the rms linewidth are discontinuous, indicating a significant change in the static local magnetic field distribution at the proton sites on traversing the PM to AFI phase transition.

The origin of these features is attributed to the large dipolar field from the 3d Fe^{3+} electron moments (spin $S_d = 5/2$, $g \approx 2$) at the proton sites, and the main features of the spectra are successfully modeled with a mean field model.

The value for J_{dd} between two nearest neighbor Fe^{3+} ions obtained from this experiment is ~ -0.85 K, which is close to the theoretical predictions.²²

It is suggested that the smaller features of the spectra that are not covered by this model are caused by the electron-electron interactions that are beyond the scope of this paper.

Acknowledgments

This work is supported at UCLA by NSF Grant DMR-0334869 (WGC) and 02030806 (SEB), partial support at NHMFL by NSF under cooperative agreement DMR-0084173, and that at Indiana by Petroleum Research fund ACS-PRF 33912-AC1. We thank A. Kobayashi and H. Kobayashi for the crystal structure data, and thank G. Gaidos, F. Zamborszky, J. Shinagawa, and F. Zhang for helpful discussions.

¹ S. Uji, H. Kobayashi, L. Balicas, and J. S. Brooks, *Adv. Mater.* **14**, 243 (2002).

² S. Uji, H. Shinagawa, T. Terashima, T. Yakabe, Y. Terai, M. Tokumoto, A. Kobayashi, H. Tanaka, H. Kobayashi, *Nature* **410**, 908 (2001).

³ H. Kobayashi, H. Tomita, T. Naito, A. Kobayashi, F. Sakai, T. Watanabe, P. Cassoux, *J. Am. Chem. Soc.* **118**, 368 (1996).

⁴ M. Tokumoto, T. Naito, H. Kobayashi, A. Kobayashi, V.

N. Laukhin, L. Brossard, P. Cassoux, *Synth. Met.* **86**, 2161 (1997).

⁵ L. Brossard, R. Clerac, C. Coulon, M. Tokumoto, T. Ziman, D. K. Petrov, V. N. Laukhin, M. J. Naughton, A. Audouard, F. Goze, A. Kobayashi, H. Kobayashi, and P. Cassoux, *Eur. Phys. J. B* **1**, 439 (1998).

⁶ H. Akutsu, E. Arai, H. Kobayashi, H. Tanaka, A. Kobayashi, and P. Cassoux, *J. Am. Chem. Soc.* **119**, 12681 (1997).

⁷ H. Kobayashi, H. Tomita, T. Udagawa, T. Naito, and A. Kobayashi, *Synthetic Metals* **70**, 867 (1995).

⁸ H. Kobayashi, E. Fujiwara, H. Fujiwara, H. Tanaka, H. Akutsu, I. Tamura, T. Otsuka, A. Kobayashi, M. Tokumoto and P. Cassoux, *J. Phys. Chem. Solids* **63**, 1235 (2002).

⁹ V. Jaccarino and M. Peter, *Phys. Rev. Lett.* **9**, 290 (1962).

¹⁰ L. Balicas, J. S. Brooks, K. Storr, S. Uji, M. Tokumoto, H. Tanaka, H. Kobayashi, A. Kobayashi, V. Barzykin, and L. P. Gor'kov, *Phys. Rev. Lett.* **87**, 067002 (2001).

¹¹ L. Balicas, V. Barzykin, K. Storr, J. S. Brooks, M. Tokumoto, S. Uji, H. Tanaka, H. Kobayashi, and A. Kobayashi, *Phys. Rev. B* **70**, 092508 (2004).

¹² P. Fulde and R. A. Ferrell, *Phys. Rev. A* **135**, 550 (1964); A. I. Larkin and Yu. N. Ovchinnikov, *Sov. Phys. JETP* **20**, 762 (1965).

¹³ M. Houzet, A. Buzdin, L. Bulaevskii, and M. Maley, *Phys. Rev. Lett.* **88**, 227001 (2002); L. N. Bulaevskii, *Sov. Phys. JETP* **38**, 634 (1974).

¹⁴ H. Akutsu, K. Kato, E. Ojima, H. Kobayashi, H. Tanaka, A. Kobayashi, and P. Cassoux, *Phys. Rev. B* **58**, 9294 (1998).

¹⁵ H. Akutsu, K. Kato, E. Arai, H. Kobayashi, A. Kobayashi, M. Tokumoto, L. Brossard and P. Cassoux, *Solid State Communications* **105**, 485 (1998).

¹⁶ H. Kobayashi, A. Kobayashi, F. Sakai, and P. Cassoux, *Chem. Soc. Rev.* **29**, 325 (2000).

¹⁷ L. K. Montgomery, T. Burgin, T. Miebach, D. Dunham, and J. C. Huffman, *Mol. Cryst. Liq. Cryst.* **284**, 73 (1996).

¹⁸ W. G. Clark, Guoqing Wu, P. Ranin, L. K. Montgomery, and L. Balicas, *Appl. Magn. Reson.* **27**, 279 (2004).

¹⁹ W. G. Clark, M.E. Hanson, F. Lefloch, and P. Ségransan, *Rev. Sci. Instrum.* **66**, 2453 (1995).

²⁰ C. P. Slichter, *Principles of Magnetic Resonance* (Springer, Berlin, 1989), 3rd ed..

²¹ A. Abragam, *The Principles of Nuclear Magnetism* (Clarendon Press, Oxford, 1962).

²² T. Mori and M. Katsuhara, *J. Phys. Soc. Jpn.* **71**, 826 (2002).

²³ N. W. Ashcroft and N. D. Mermin, *Solid State Physics* (Holt, Rinehart and Winston, New York, 1976), 1st ed..

²⁴ C. Hotta and H. Fukuyama, *J. Phys. Soc. Jpn.* **69**, 2577 (2000).

²⁵ G. C. Carter, L. H. Bennett, and D. J. Kahan *Metallic Shifts in NMR* (Pergamon, London, 1977), part I.

²⁶ J. D. Jackson, *Classical Electrodynamics* (John Wiley & Sons, Singapore, 1990), 2nd ed..

²⁷ G. B. Arfken and H. J. Weber, *Mathematical Methods for Physicists* (Academic Press, Inc., San Diego), 4th ed..

²⁸ The Lorentz field B^{Lor} and demagnetization field B^{dem} in λ -(BETS)₂FeCl₄ can be expressed respectively as, $B^{\text{Lor}} = \frac{4\pi}{3} \frac{M(x)}{N_A v_{Fe}}$ and $B^{\text{dem}} = 4\pi D \frac{M(x)}{N_A v_{Fe}}$, where D is the demagnetization factor depending on sample size, $M(x)$ is the magnetization of the 3d Fe³⁺ electrons, N_A is the Avogadro number, v_{Fe} is the unit cell volume per Fe³⁺ ion, and B_0 is the applied magnetic field. Here $D \approx 0.1$ according to the size of the needle shape single crystal.

²⁹ Guoqing Wu, P. Ranin, and W. G. Clark, unpublished.

³⁰ M. Watanabe, S. Komiyama, R. Kiyanagi, Y. Noda, E. Negishi and N. Toyata, *J. Phys. Soc. Jpn.* **72**, 452 (2003).